Chapter 14B. Analysis of Imaging Spectrometer Data for the Tourmaline Area of Interest

Contribution by Trude V.V. King

Abstract

Computer analysis of the HyMap spectroscopic data of the Tourmaline area of interest (AOI) in the west-central part of Afghanistan used spectrum matching techniques to identify the occurrence of selected surficial minerals based on characteristic absorption features (absorption bands) in the HyMap data compared to a library of spectral standards. This area is spectrally very complex with many examples of alluvial fans, intrusions, mineralized zones, and obvious fault traces.

Carbonate minerals and mineral mixtures cover most of the AOI. However, iron oxides and iron hydroxides are present and suggest areas of oxidation of surficial minerals. The four known vein tin mineral occurrences are located in the northern portion of the AOI and are associated with serpentines and muscovites.

In the central portion of the AOI, the presence and combined occurrence of buddingtonite, hydrated silica, jarosite, and kaolinite suggest extensive areas of advanced argillic alteration, which is commonly associated with gold and porphyry deposits. The mineralized area occurs in a northeast-trending fault-bound region in Eocene-Oligocene age rocks. The predominant minerals in the fault bounded region are iron hydroxides and goethites with lesser amounts of Fe^{3+} minerals.

A number of topographic highs bounded by hematitic minerals in the central part of the AOI delineate previously unrecognized intrusive bodies. Other circular or nearly circular features that may be intrusions occur in the northeast corner, along the northern boundary (near the center), and the southwest corner of the AOI.

Bedded rocks are present in the Barremian-Aptian age rocks in the southeast corner of the AOI. The mineral distribution maps suggest an area of intrusions, bedded units, and terraces of weathered surficial material. The HyMap data show a complex, compositionally varied mineral distribution pattern.

14B.1 Introduction

Previous U.S. Geological Survey (USGS) analyses of existing geologic data of Afghanistan revealed numerous areas with indications of potential mineral resources of various types (Peters and others, 2007). Several of these were selected for studies using hyperspectral remote sensing (imaging spectroscopy) data to characterize surface materials. One of those areas is the Tourmaline area of interest (AOI) in central Afghanistan. The Tourmaline AOI is approximately 690 km west and south of Kabul (fig. 14B–1) and potentially contains tin- and tungsten-vein, stockwork, and greisen or porphyry tin deposits. To help assess these potential resources, high-resolution hyperspectral data were analyzed to detect the presence of selected minerals that may be indicative of past mineralization processes. This report contains the results of those analyses and identifies numerous sites within the Tourmaline AOI that merit further investigation, especially detailed geological mapping and geochemical analysis.

14B.2 Data Collection and Processing

In 2007, imaging spectrometer (hyperspectral) data were acquired over most of Afghanistan as part of the USGS “Oil and Gas Resources Assessment of the Katawaz and Helmand Basins” project. These data were collected to characterize surface materials in support of assessments of resources (coal, water, minerals, and oil and gas) and earthquake hazards in the country (King and others, 2010).

Imaging spectrometers measure the reflectance of visible and near-infrared light from the Earth's surface in many narrow channels, producing a reflectance spectrum for each image pixel. These reflectance spectra can be interpreted to identify absorption features that result from specific chemical transitions and molecular bonds that provide compositional information about surface materials. Imaging spectrometer data can only be used to characterize the upper surface materials and not subsurface composition or structure. However, the results of subsurface processes can be indicated by the distribution of surface materials that can be detected using hyperspectral (imaging spectroscopy) data.

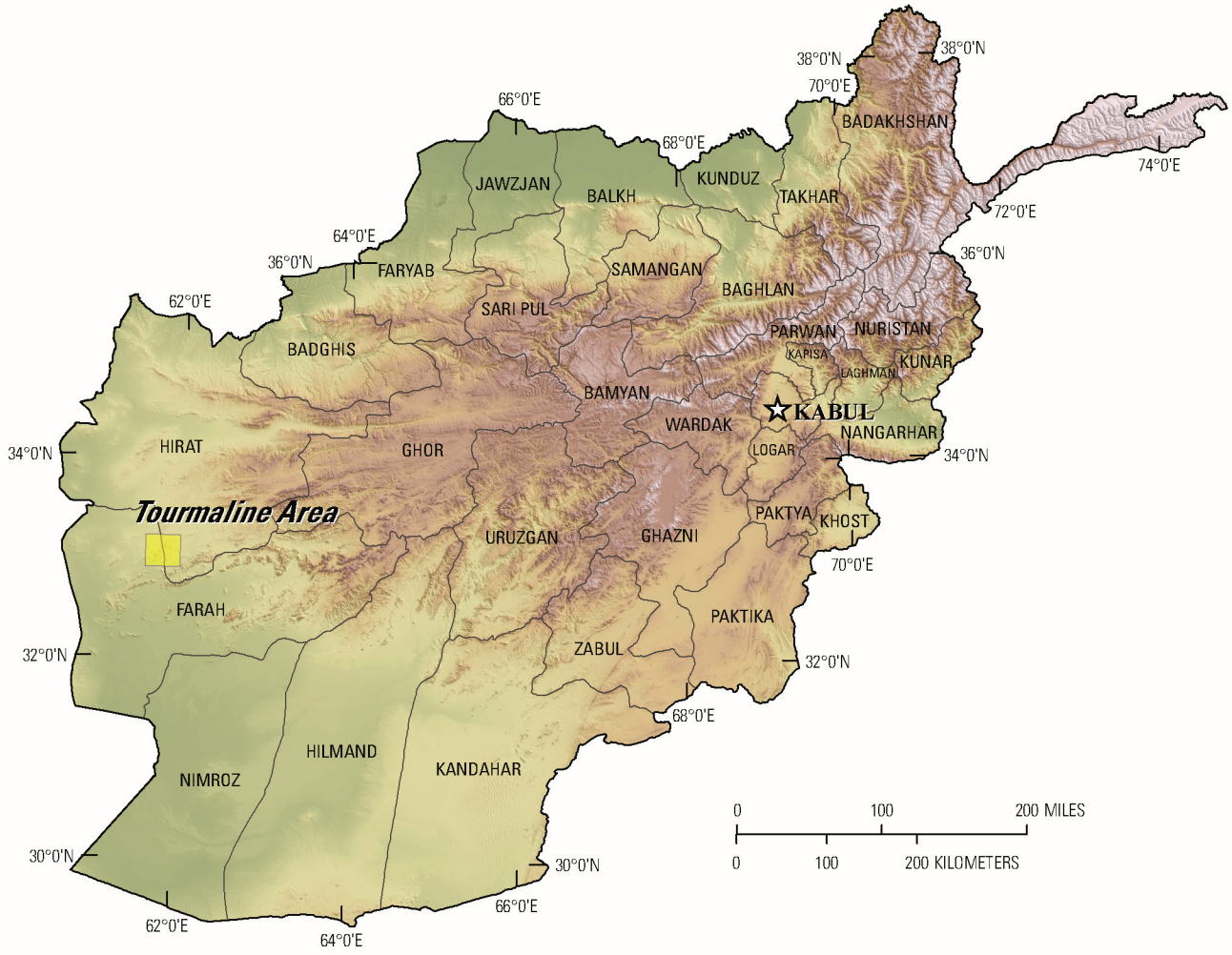

Figure 14B–1. The Tourmaline area of interest is located approximately 690 kilometers west and south of Kabul in the Farah and Herat Provinces of Afghanistan.

14B.2.1 Collection of Imaging Spectrometer Data

The HyMap imaging spectrometer (Cocks and others, 1998) was flown over Afghanistan from August 22 to October 2, 2007 (Kokaly and others, 2008). HyMap has 512 cross-track pixels and covers the wavelength range 0.43 to 2.48 micronmeterss (μm) in 128 channels. The imaging spectrometer was flown on a WB-57 high-altitude aircraft at approximately 50,000 ft. There were 207 standard data flight lines and 11 cross-cutting calibration lines collected over the country of Afghanistan for a total of 218 flight lines, covering a surface area of 438,012 km^2 (Kokaly and others, 2008). Data were received in scaled radiance format (calibrated to National Institute of Standards and Technology reference

materials). Before processing, four channels that had low signal-to-noise ratios and (or) were in wavelength regions overlapped by adjacent detectors were removed from the image cubes. Each flight line was georeferenced to Landsat Thematic Mapper (TM) base imagery in UTM projection (Davis, 2007).

14B.2.2 Calibration

HyMap data were converted from radiance to reflectance using a multi-step process. This calibration process removed the influence of the solar irradiance function, atmospheric absorptions, and residual instrument artifacts, resulting in reflectance spectra that have spectral features that result from the material composition of the surface. Because of the extreme topographic relief and restricted access to ground calibration sites, modifications to the typical USGS calibration procedures were required to calibrate the 2007 Afghanistan HyMap dataset (Hoefen and others, 2010). In the first step of the calibration process, the radiance data were converted to apparent surface reflectance using the radiative transfer correction program Atmospheric CORrection Now (ACORN; ImSpec LLC, Palmdale, Calif.). ACORN was run multiple times for each flight line, using average elevations in 100-m increments, covering the range of minimum to maximum elevation within the flight line. A single atmospherically corrected image was assembled from these elevation-incremented ACORN results. This was done by determining the elevation of each HyMap pixel and selecting the atmospherically corrected pixel from the 100-m increment closest to that elevation.

Each assembled atmospherically corrected image was further empirically adjusted using ground-based reflectance measurements from a ground-calibration site. Spectra of five Afghan ground-calibration sites were collected: field spectra from Kandahar Air Field, Bagram Air Base, and Mazar-e-Sharif Airport, as well as, laboratory spectra of soil samples from two fallow fields in Kabul. These were used to calculate empirical correction factors using the pixels of atmospherically corrected HyMap data in the flight lines that passed over the sites. The empirical correction from the closest calibration site to each flight line was applied.

To further improve the data quality, an additional calibration step was taken to address the atmospheric differences caused, in part, by the large distances from calibration sites to where the HyMap data were acquired. The large distances were a result of the lack of safe access to ground-calibration sites. The duration of the airborne survey and variation in time of day during which flight lines were acquired also resulted in differences in atmospheric conditions between standard flight lines and lines over ground-calibration sites, which were used to derive the empirical correction factors. Over the course of the data collection, the sun angle, atmospheric water vapor, and atmospheric scattering differed for each flight line. To compensate for this, cross-cutting calibration flight lines over the ground-calibration areas were acquired (Kokaly and others, 2008) and used to refine data quality of standard data lines. A multiplier correction for each standard data line, typically oriented north-south, was derived using the pixels of overlap with the well-calibrated cross-cutting line that intersected it, subject to slope, vegetation cover, and other restrictions on pixel selection (Hoefen and others, 2010). As a result, the localized cross-calibration multiplier, derived from the overlap region, corrected residual atmospheric contamination in the imaging spectrometer data that may have been present after the ground calibration step.

14B.2.3 Materials Maps and Presentation

After the calibration process, the reflectance data were georeferenced and then analyzed using Material Identification and Characterization Algorithm (MICA), a module of the USGS Processing Routines in IDL for Spectroscopic Measurements (PRISM) software (Kokaly, 2011). MICA compared the reflectance spectrum of each pixel of HyMap data against entries in a reference spectral library of minerals, vegetation, water, and other materials. The library included 97 reference spectra of

well-characterized mineral and material standards. The resulting maps of material distribution, resampled to a 23×23-m^2 pixel grid, were used to prepare maps of mineral, vegetation, and other material occurrences.

MICA was applied to HyMap data twice to present the distribution of two categories of minerals that are naturally separated in the wavelength regions of their primary absorption features. MICA was applied using the subset of minerals with absorption features in the visible and near-infrared wavelength region, producing a 1-µm map of iron-bearing minerals and other materials (King, Kokaly, and others, 2011), and again using the subset of minerals with absorption features in the shortwave infrared, producing a 2-µm map of carbonates, phyllosilicates, sulfates, altered minerals, and other materials (Kokaly and others, 2011). For clarity of presentation, some individual classes in these two maps were bundled by combining selected mineral types (for example, all montmorillonites or all kaolinites) and representing them with the same color in order to reduce the number of colors required to represent the mineral classes.

The iron-bearing minerals map has 28 classes. Iron-bearing minerals with different mineral compositions but similar spectral features are difficult to classify as specific mineral species. Thus, generic spectral classes, including several minerals with similar absorption features, such as Fe^{3+} Type 1 and Fe^{3+} Type 2 are depicted on the map. The carbonate, phyllosilicates, sulfates, and altered minerals map has 32 classes. Minerals with slightly different mineral compositions but similar spectral features are less easily discriminated; thus, some identified classes consist of several minerals with similar spectra, such as the chlorite or epidote class. When comparisons with reference spectra produced no viable match, a designation of "not classified" was assigned to a pixel.

14B.2.4 Data Limitations

It should be noted that geographic registration between various datasets is not always possible because of differences in collection methods and resolution. The geographic accuracy and quality of each dataset are limited by the original source. Significant efforts were made to ensure the geographic accuracy of the HyMap data (Kokaly and others, 2008; Hoefen and others, 2010). However, exact registration between previously published known mineral occurrences, fault traces, geologic units, and structural boundaries in comparison to the HyMap data may not be ideal. To resolve additional details, the digital versions of these maps can be viewed at higher spatial resolution than what is possible in a single-page printed map.

14B.3 Geologic Setting of the Tourmaline AOI

The Tourmaline AOI is located in the Farah and Hirat Provinces of Afghanistan (fig. 14B–1). Elevations in the AOI range from 881 to 1,830 m (fig. 14B–2). The contrast-enhanced natural color composite of Landsat Thematic Mapper bands in figure 14B–3 provides a general overview of the Tourmaline AOI terrain and is useful for understanding the general characteristics and distribution of surficial material including rocks and soil, unconsolidated sediments, vegetation, and hydrologic features. Stratified rocks in the AOI range in age from Valanginian-Hauterivian to Recent and a single Oligocene intrusion is also present (fig. 14B–4; Doebrich and others, 2006; Abdullah and Chmyriov, 1977). There are four known vein tin occurrences and five northeast- to southwest-trending fault traces in the area (fig. 14B–5).

Figure 14B–5 shows the locations of potential areas of mineralization based on reconnaissance field geology and the geologic literature. Two of the occurrences (Kuchi and Bulgaja) occur along a fault and two occurrences (unnamed) have no associations with known faulting (fig. 14B–5). The Bulgaja occurrence lies in a silicified, serpentinized, brecciated shear zone and contains tin with traces of lead and zinc. The Kuchi occurrence is hosted in Oligocene granite and is composed of silicified felspathized zones, which are reported to contain tin, copper, zinc, and lead (V.N. Efimenko and others, Afghanistan Department of Geological and Mineral Survey, unpub. data, 1973). The known mineralized

locations are summarized in table 1. The widespread occurrence of altered rocks and the tin contents of collected field samples (Peters, chap. 14A, this volume) indicate that this area could contain one or more large tin-vein, stockwork, or porphyry deposits.

14B.4 Mineral Maps of the Tourmaline Area of Interest

Analysis of the HyMap imaging spectrometer data of the Tourmaline AOI using spectroscopic methods resulted in the identification of a wide variety of minerals exposed at the surface. Although the occurrence of certain minerals may suggest that mineralization processes may have once operated in the area, many of the minerals that were identified are also common rock-forming minerals or minerals that can be derived from the weathering of a wide variety of rock types. Consequently, the distribution patterns of the identified minerals and the geologic context in which they occur are extremely important in understanding the causes of mapped mineral occurrences and evaluating the possible potential for related mineral deposits.

Figures 14B–6 and 14B–7 show the distribution of the iron-bearing minerals (28 possible classes) and carbonates, phyllosilicates, sulfates, and other alteration minerals (32 possible classes) for the Tourmaline AOI. To enhance visualization of the subtleties of the mineral distribution patterns in these classified image maps, a series of topical images depicting groups of minerals that are commonly related or occur together in special geologic environments has been produced. Figure 14B–8 shows the distribution of carbonate minerals in the AOI, and figure 14B–9 shows where the clays and micas were mapped. The distribution of iron oxide and iron hydroxide minerals are shown in figure 14B–10. Secondary minerals are shown in figure 14B–11, and minerals commonly found in hydrothermally altered rocks are shown in figure 14B–12.

14B.4.1 Carbonate Minerals

The calcite + muscovite/illite and calcite mineral groups cover more than 90 percent of the mapped area and are continuous across geologic boundaries (fig. 14B–8). Dolomite and dolomite mixtures are widely scattered and are present throughout the area. Spatially consistent patterns of iron-bearing carbonates occur adjacent to or south of the major fault in the southernmost part of the AOI.

14B.4.2 Clays and Micas

Muscovites and illites are the most abundant minerals groups (fig. 14B–9) mapped in the AOI. Although the muscovite and illite minerals have been mapped over the entire area, the spatially distinct pixels of muscovite are more common in the Eocene-Oligocene rocks. The chlorite and epidote group, illites, and epidote minerals commonly occur in the older Barremian-Aptian and Valanginian-Hauterivian rocks. A small cluster of chlorite or epidote pixels are mapped in an outlier of Valanginian-Hauterivian rocks that appear as a topographic high in the southern part of the area. The Kuchi known mineral occurrence is surrounded by pixels of muscovite-rich material.

The montmorillonite group of minerals occur throughout the area but somewhat more concentrated south of lat 33°10′0″ N. Small clumps of montmorillonite are present in the late Quaternary and Recent rocks in the southern part of the AOI.

Pixels mapped as kaolinite minerals preferentially occur in the Eocene-Oligocene rocks. The pockets of kaolinite minerals occur near fault traces in the Eocene-Oligocene rocks and are mixed with muscovites.

14B.4.3 Iron Oxides and Hydroxides

Figure 14B–10 shows the occurrence of iron oxides and iron hydroxides in the Tourmaline AOI. This image illustrates the complex geologic, tectonic, and alteration processes that have occurred in the

area. On the basis of the HyMap data, the Eocene-Oligocene rocks appear to have experienced multiple intrusions and faulting (center portion of the AOI). None of the known mineral occurrences are associated with minerals mapped in this image.

The dark areas in the image (where no minerals were identified in this topical map) correspond to topographic highs that are characterized by pixels of calcite and dolomite minerals and mineral groups (fig. 14B–8). These nine zones occur near a mapped fault that cuts the Eocene-Oligocene rocks; a smaller nearly circular feature occurs in the northeastern part of the Eocene-Oligocene unit. Mineral distribution patterns on either side of the fault are notable as each area has the potential to host economically important mineral deposits. The area on the south side of the chain of intrusions is dominated by the presence of hematitic minerals that appear to represent both isolated lithologically controlled concentrations of hematite (such as the two spatially coherent groups of hematite pixels in the Eocene-Oligocene rocks that occur near lat 33° N., long 61°55′ E.) and hematitic weathering products that form large alluvial fans.

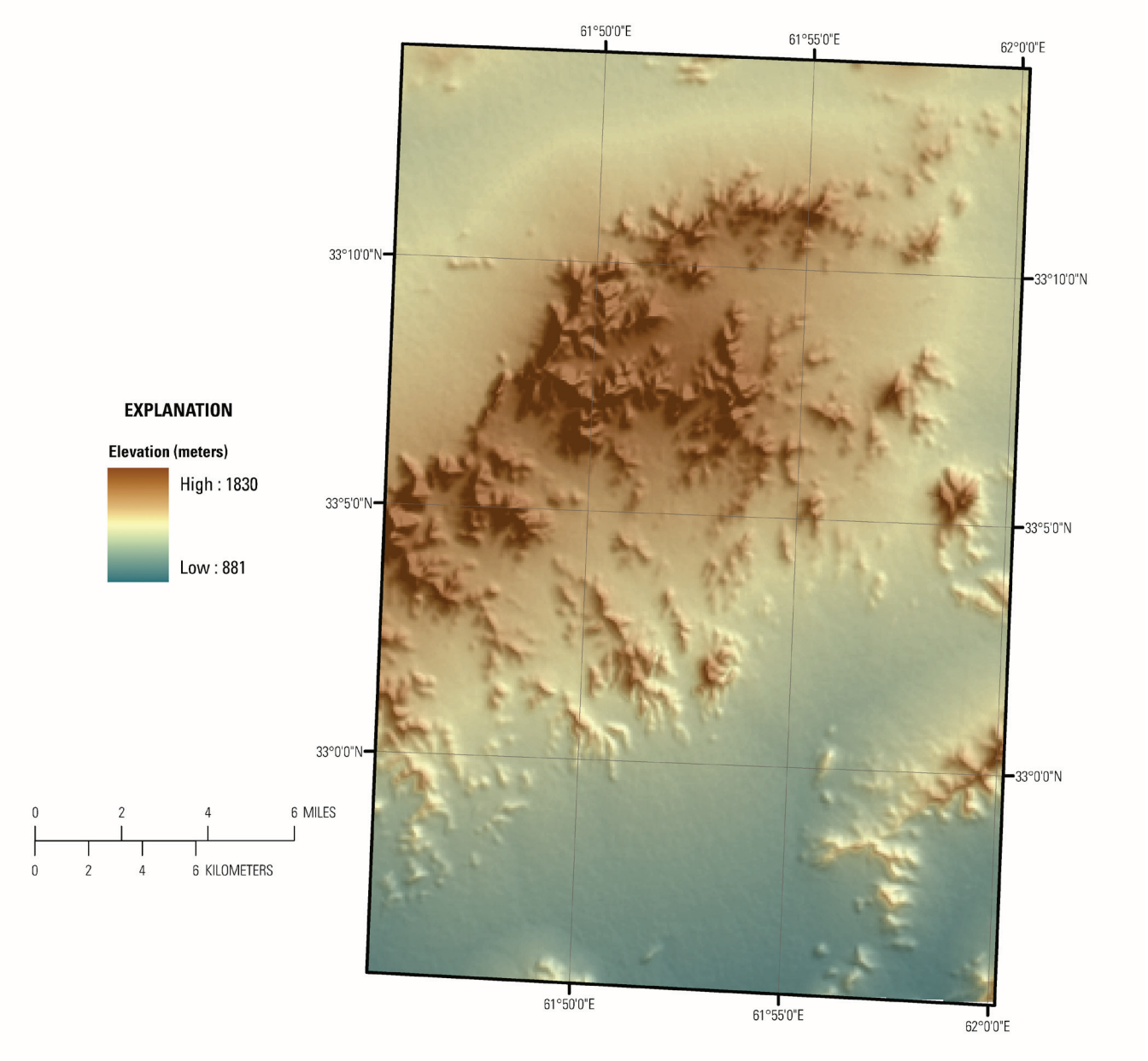

Figure 14B–2. Shaded relief map showing elevations in the Tourmaline area of interest. The darker brown tones indicate the higher elevations and the lower elevations are represented by the blue tones.

Mineralization in the area immediately to the north of the intrusive chain, bounded by two fault traces, is dominated by the presence of goethitic and iron hydroxide minerals. Hematitic and goethitic minerals are also found in the northwest corner of the image in Eocene-Oligocene and Pliocene age rocks and in alluvial fans in the late Quaternary and Recent geologic units.

The iron-oxides and iron-hydroxides map for the Tourmaline AOI was used as the primary tool to identify fourteen new sites of potential mineralization (King, Johnson, and others, 2011).

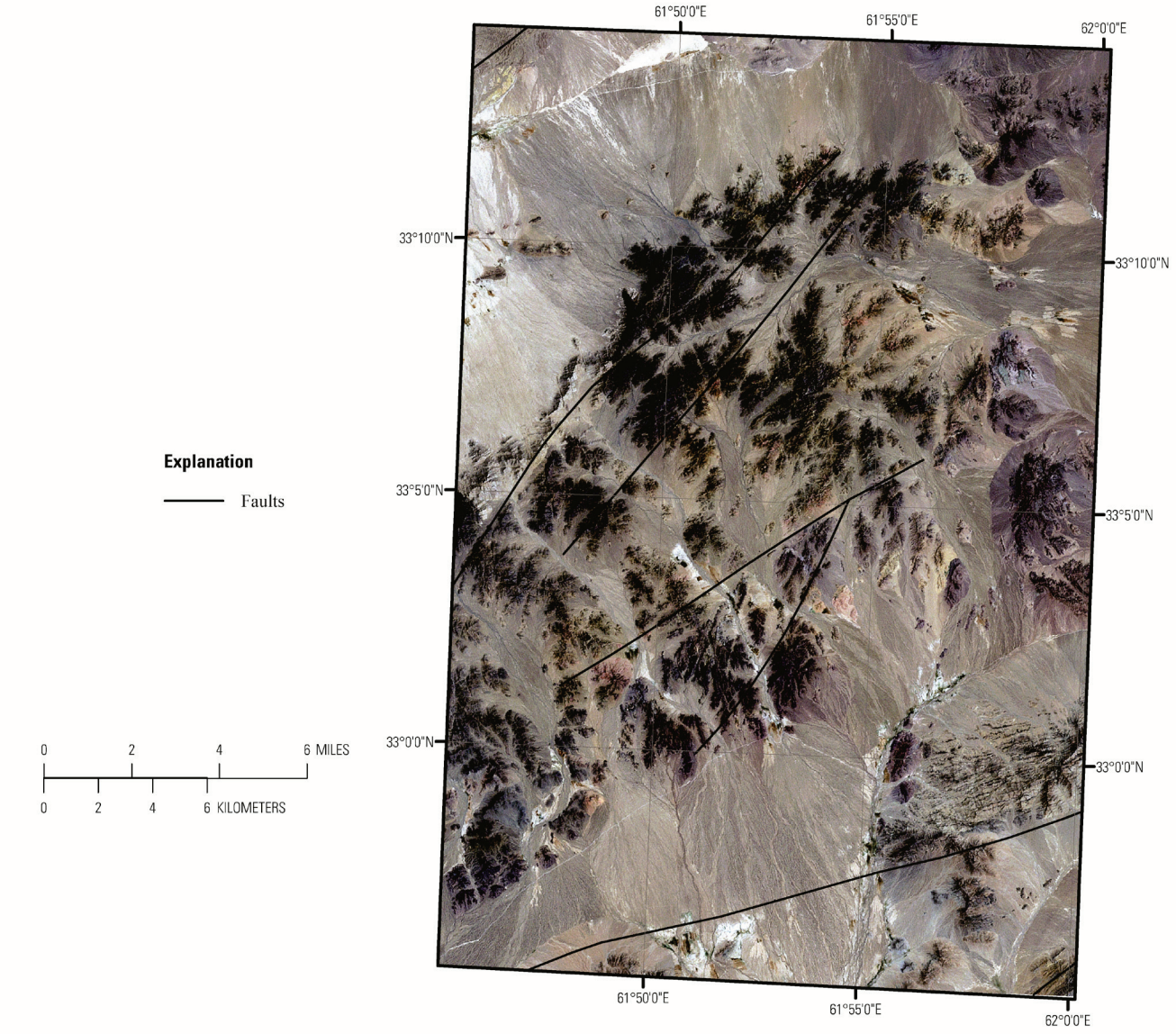

Figure 14B–3. Five northeast-southwest trending fault traces are present in the Tourmaline area of interest. The fault traces (Peters and others, 2007) are shown on Landsat Thematic Mapper (TM) base imagery (Davis, 2007).

14B.4.4 Common Secondary Minerals

The occurrence and distribution of common secondary minerals for the AOI are shown in figure 14B–11. The Bulgaja mineral occurrence site is characterized by the presence of serpentine group minerals and agrees with the alteration type included in table 1. Other mineral occurrences in the AOI (Kuchi and two unnamed locations) have lesser amounts of serpentine minerals with some epidote or

chlorite or epidote mapped. Chlorite and chlorite or epidote minerals map in the southeast corner and south-central portion of the AOI in the Lower Cretaceous (Valanginian-Hauterivian) units.

14B.4.5 Common Alteration Minerals

Most of the minerals in this group are commonly present in hydrothermally altered rocks associated with epithermal processes. Consequently, where they occur in distinct clusters is of great interest in terms of potential mineral deposits. The Tourmaline AOI shows widespread distribution of minerals and suites of minerals and patterns of alteration that indicate potentially large mineral occurrences (fig. 14B–12). Abdullah and others (1977) and Peters and others (2007) suggest that the area could contain one or more large tin-vein, stockwork, or porphyry deposits. The two unnamed prospects show pixels of chlorite or epidote group minerals in proximity to their locations. However, none of the known sites occur in areas that have an abundance of common alteration minerals. Thus, the primary discussion of the common alteration materials will be included in the mineral anomaly report (King, Johnson, and others, 2011), but the following overview of the findings are presented herein.

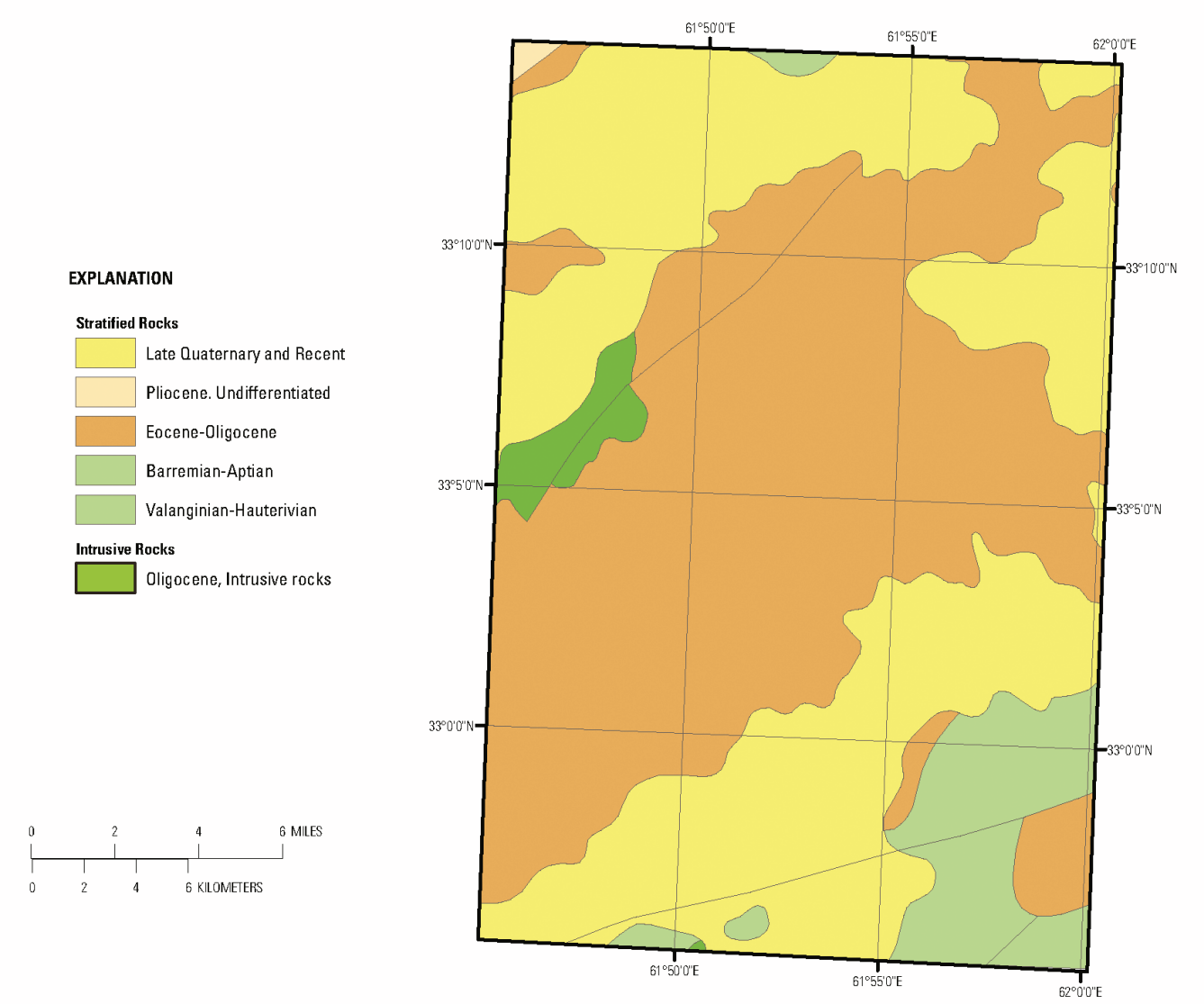

Figure 14B–4. The geologic map of the Tourmaline area of interest is taken from Doebrich and others (2006), Abdullah and others (1977) ,and Peters and others, (2007).

Kaolinite group minerals occur along and adjacent to the fault that is present in the Eocene-Oligocene rocks. The spatially coherent kaolinitic pixels indicate the southern edge of potential hydrothermal alteration. The northern bounding fault is marked by the presence of small amounts of kaolinite that occur with jarositic minerals (lat 33°7′14.80″N., long 61°51′1″E.). The identification of jarositic minerals is important as they represent a weathering product of pyrite, a primary product in the epithermal process related to ore formation. The fault-bounded region includes spatially isolated pixels of jarositic minerals and hydrated silica. Jarositic minerals are discontinuously located along a trend that stretches from lat 33°1′25.41″ N., long 61°48′40.695″ E., to lat 33°8′41.90″ N., long 61°54′34.77″ E. Hydrous silica occurs in association with jarosite at lat 33°6′6.79″ N., long 61°52′36.67″ E. (fig. 14B–12). This spatially coherent assemblage of minerals warrants detailed field examination and geochemical sampling as hydrous silica is commonly the uppermost expression of a hydrothermal system.

Buddingtonite, a methane-bearing mineral, commonly associated with hydrothermal mineral processes, is mapped in two locations (near lat 33°6′6.79″ N., long 61°52′36.67″ E.) in the contact zone between the Eocene-Oligocene rocks and the late Quaternary and Recent geologic unit to the south.

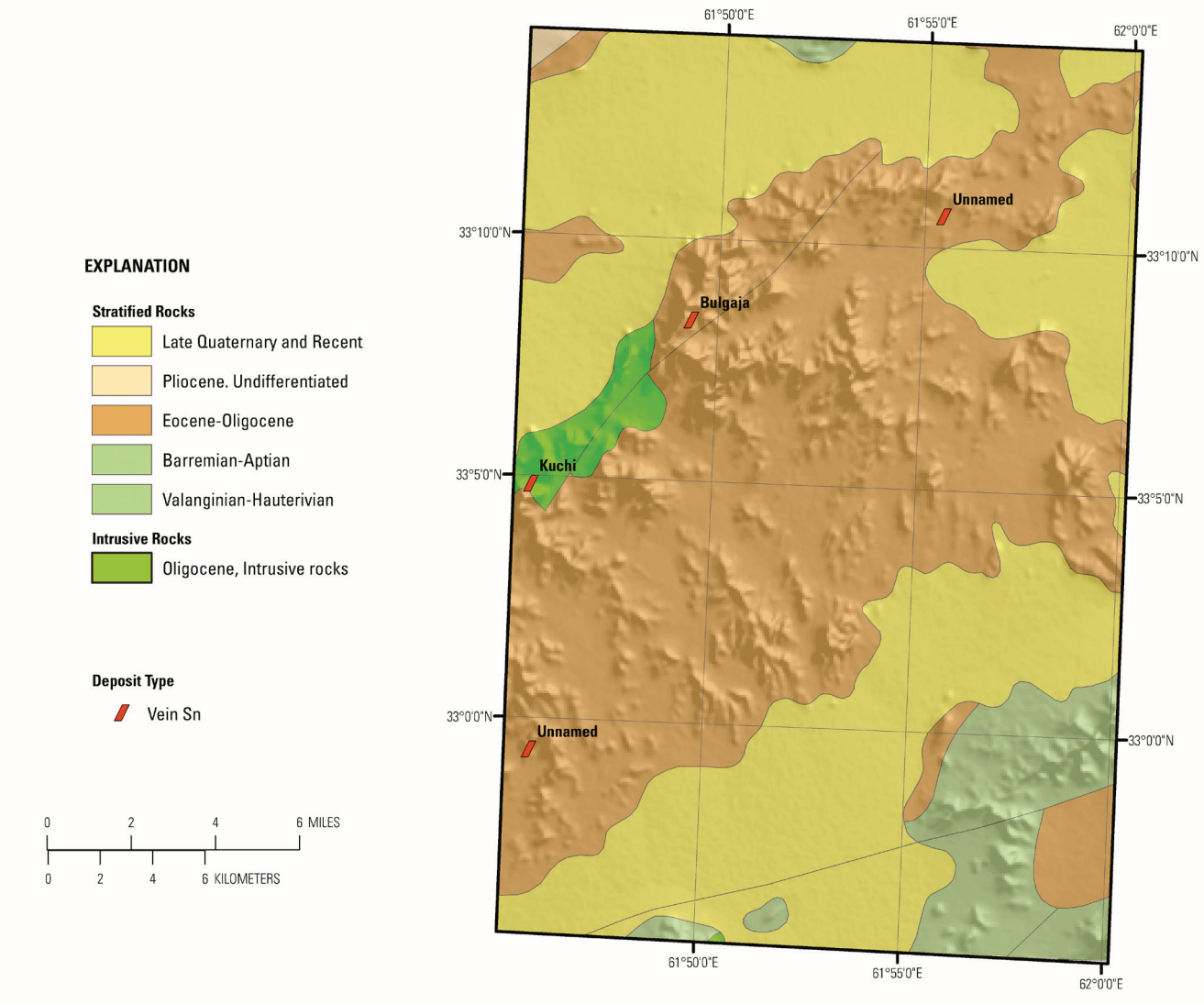

Figure 14B–5. Location of known mineral occurrences in the Tourmaline area of interest. The map consists of four data layers: shaded relief base map, transparency of the geologic map (Doebrich and others, 2006; Abdullah and others, 1977), fault traces (Peters and others, 2007), and known mineral occurrences (Peters and others, 2007).

14B.5 Summary

The Kuchi and Bulgaja tin occurrences are shown to be related to minerals and suites of minerals that define their known alteration mineralogy (table 14B–1). The Kuchi prospect is spatially correlated with distinct pixels of clays and micas but shows no correlation with minerals mapped in the other topical maps. The Bulgaja prospect overprinted serpentinization is detected and mapped in the HyMap data by the spatially related pixels of serpentine and serpentine group minerals.

The mapped minerals, mineral groups, and their spatial relations suggest that the AOI is a favorable environment to host nonfuel mineralization. The presence and combination of buddingtonite, hydrated silica, jarosite, and kaolinite suggest extensive areas of advanced argillic alteration, which is associated with gold and porphyry mineralization. The HyMap data show several occurrences of buddingtonite (lat 33°0′30.56″ N., long 61°53′11.37″ E.). Figure 14B–13 shows a 3D projection of the buddingtonite (yellow pixels) occurrence. In addition, a series of jarosite-goethite-hematite occurrences extend diagonally across the image (lat 33°7′7.19″ N., long 61°56′56.46″ E., to lat 33°1′25.42″ N., long 61°48′40.695″ E.) covering an area approximately 15 km in length. These advanced argillic mineral assemblage areas occur between two semiparallel bounding fault traces in Eocene-Oligocene rocks.

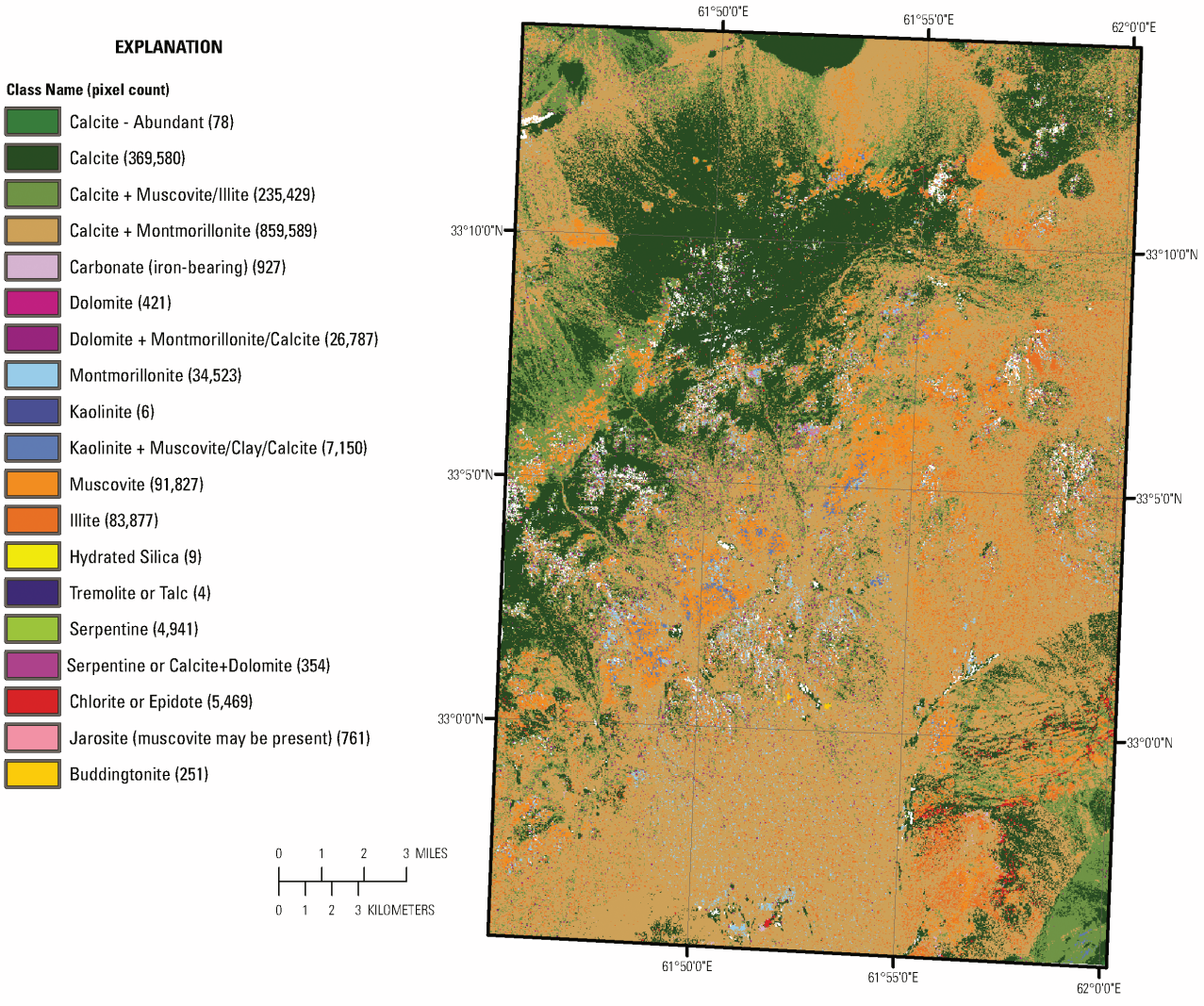

Figure 14B–6. Image showing iron-bearing and other alteration minerals in the Tourmaline area of interest that were detected in the HyMap data.

A series of topographic highs occur adjacent and south of the southern bounding-fault trace in the middle of the AOI. The only mineral groups mapped on the topographic highs are calcite and montmorillonite group minerals (fig. 14B–9). However, the HyMap (fig. 14B–10) images show hematite on the flanks and in the surficial material being eroded off the topographic highs (fig. 14B–13). Based on the mapped mineral assemblages and surficial patterns, the HyMap data suggest that these are a series of intrusive plutons. Additional semiround, topographically high areas in the northeast, north-central, and southwest parts of the AOI that are surrounded by hematitic and/or goethitic minerals may also be oxidized intrusive rocks.

Buddingtonite, a methane-bearing mineral, which is commonly associated with hydrothermal processes, is mapped in two locations (near lat 33°6′6.79″ N., long. 61°52′36.67″ E.) in the contact zone between the Eocene-Oligocene rocks and the late Quaternary and Recent geologic unit to the south. The mineral composition, number of pixels mapped, and their spatial proximity make this another target for field investigation and geochemical sampling.

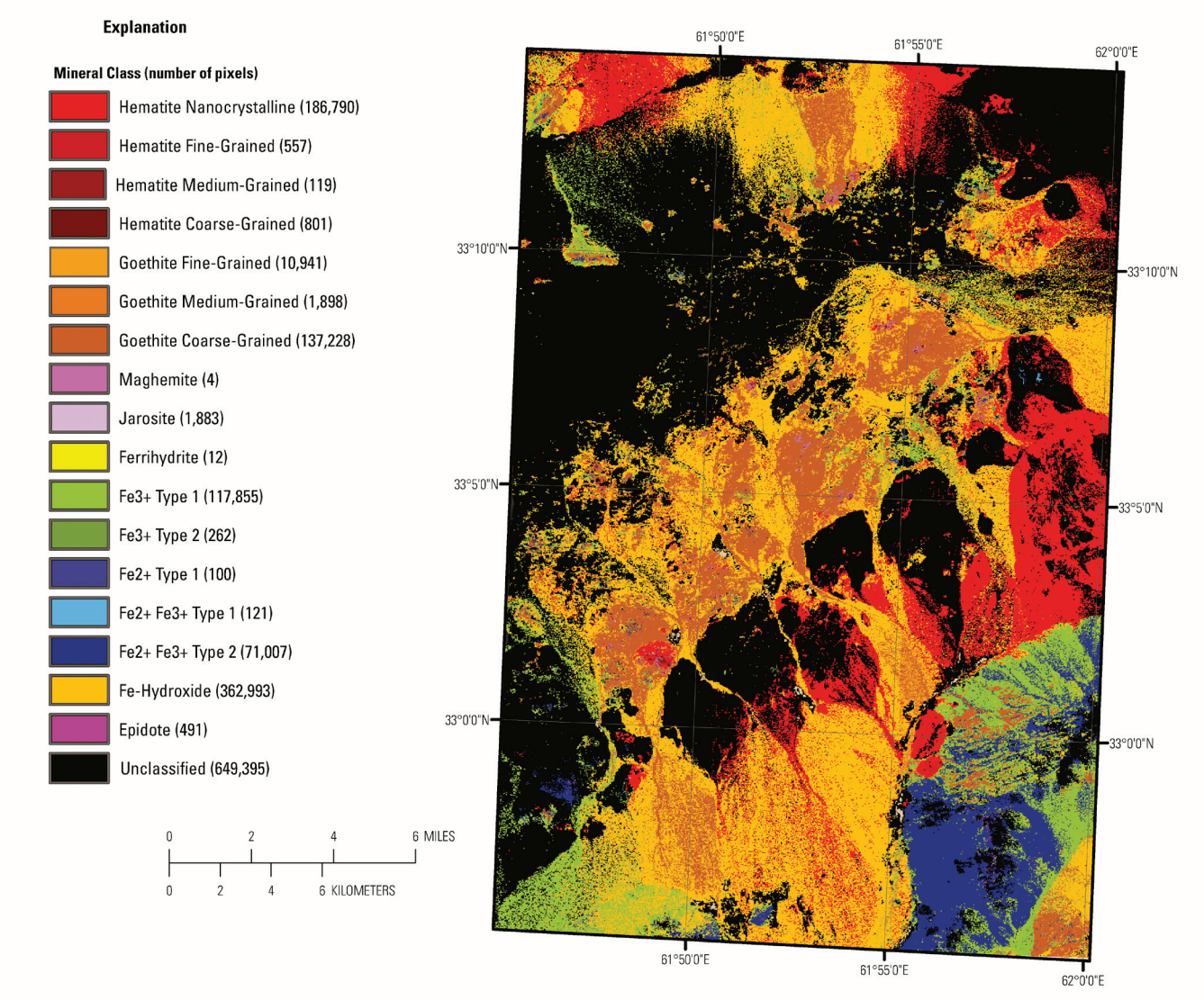

Figure 14B–7. Distribution of clays, carbonates, phyllosilicates, sulphates, and other alteration minerals for the Tourmaline area of interest as mapped by the HyMap data.

Bedded rocks are present in the Barremian-Aptian age rocks in the southeast corner of the AOI. HyMap data suggest this is an area of intrusions, bedded units, and terraces of altered surficial material

of varied origin. Fe^{2+} minerals are abundant in this part of the AOI and appear to be the weathering or alluvial material that mineralogically defines the large rounded topographic feature. The periphery of the large Fe^{2+}-rich feature has two associated areas of spatially coherent hematite pixels near the central part of the alteration pattern.

The HyMap data show complex, compositionally varied mineral assemblages and distribution patterns suggestive of extensive previous hydrothermal activity within the AOI. Potential new mineral occurrences (14 different anomalies) in the AOI are discussed in the companion anomaly database report (King, Johnson, and others, 2011).

Table 14B–1. Known mineral occurrcences in the Tourmaline area of interest.

Name	Deposit type	Mineralogy	Gangue	Alteration
Unnamed	Tin vein	Cassiterite	Tourmaline	Tourmalinization
Kuchi	Tin vein	Cassiterite	Quartz	Silicification
Bulgaja	Tin vein	Galena; hematite	Quartz; serpentine	Silicification; overprinting serpentinization
Unnamed	Tin vein	Galena; malachite; hematite	Quartz; tourmaline	Silicification; hematitization; tourmalinization

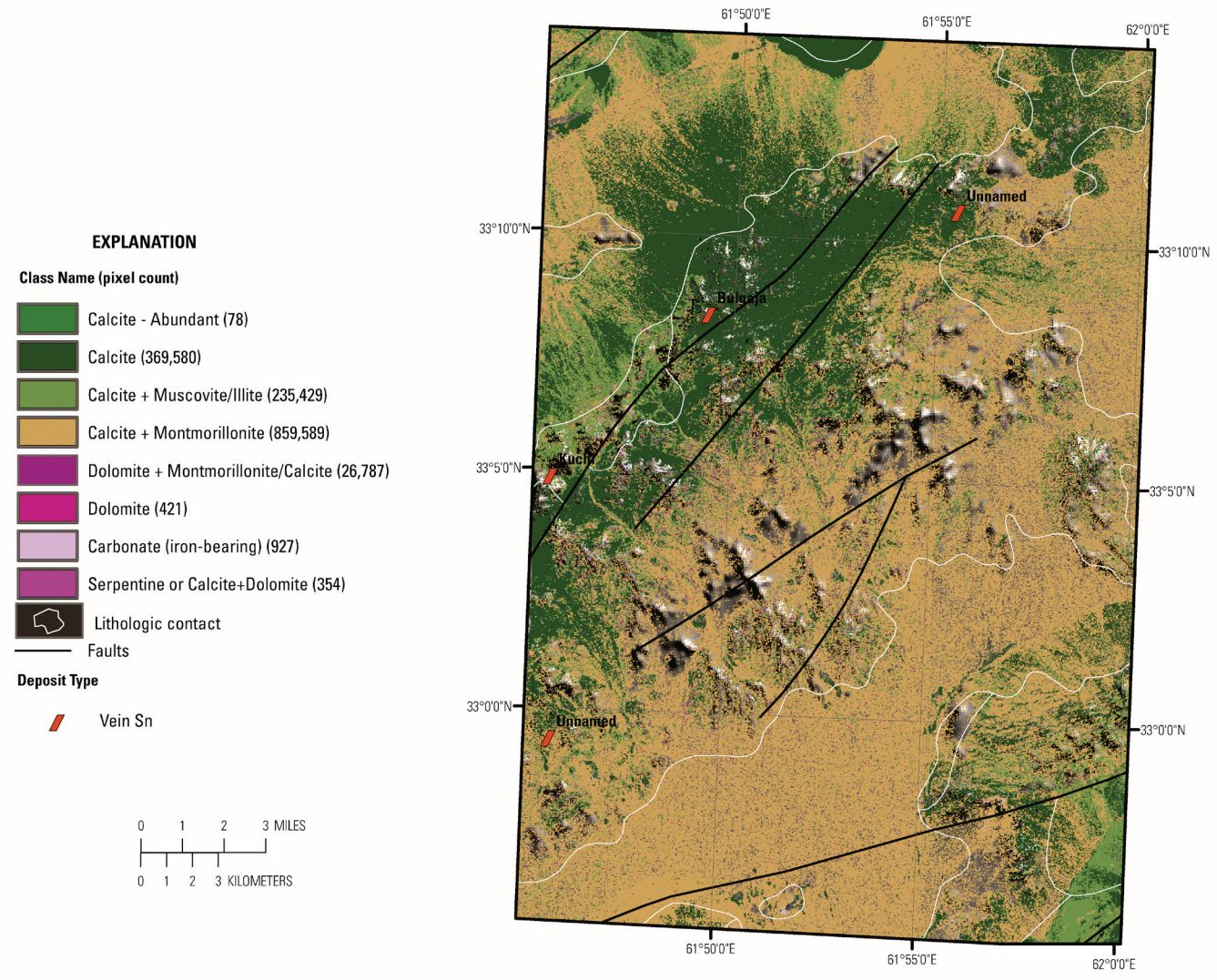

Figure 14B–8. Distribution of carbonate-bearing minerals detected by the HyMap data in the area of interest.

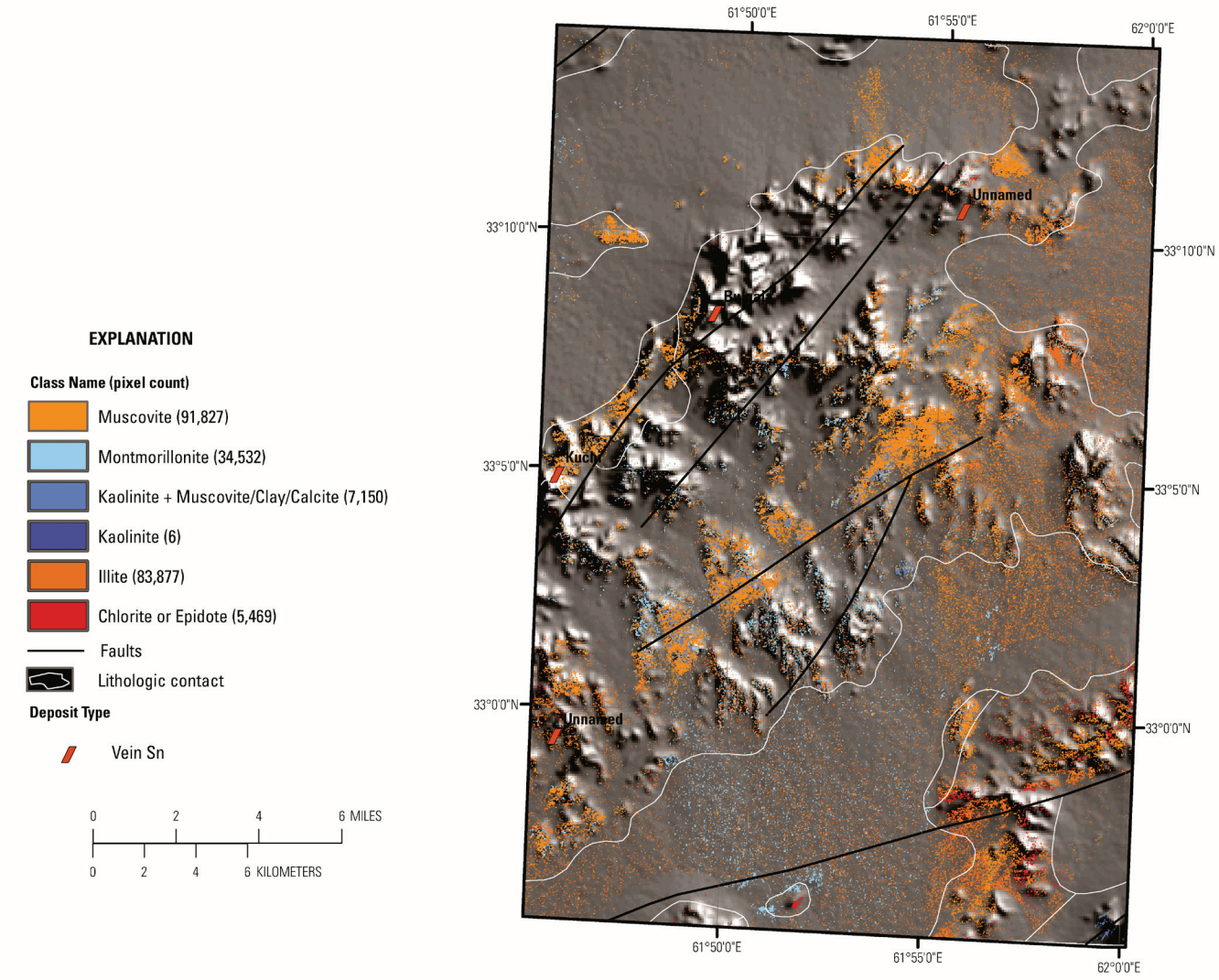

Figure 14B–9. Distribution of clays and micas identified in the HyMap data for the Tourmaline area of interest.

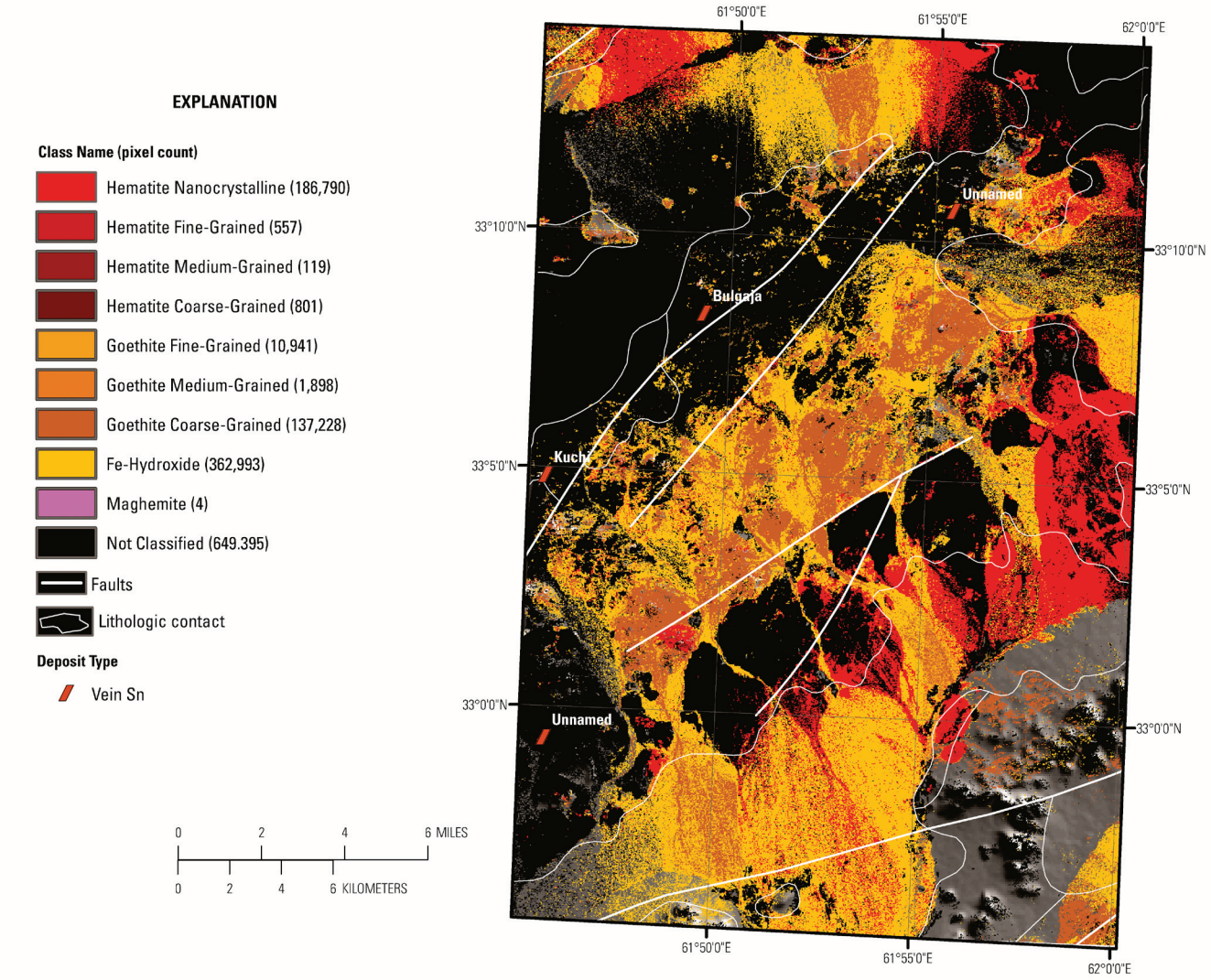

Figure 14B–10. Distribution of iron hydroxides and iron oxides mapped using the HyMap data for the Tourmaline area of interest.

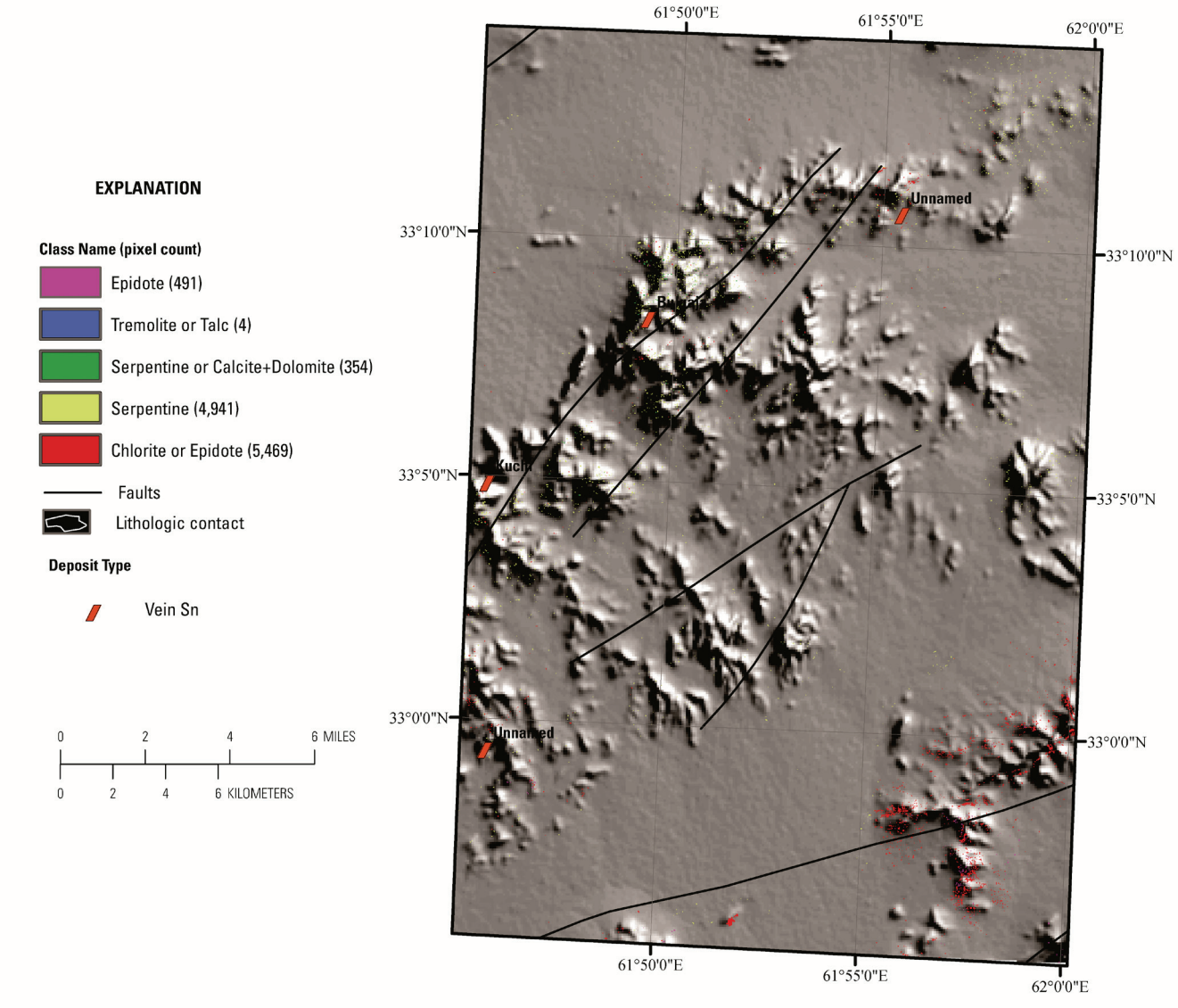

Figure 14B–11. Occurrence and distribution of common secondary minerals detected in the HyMap data for the Tourmaline AOI.

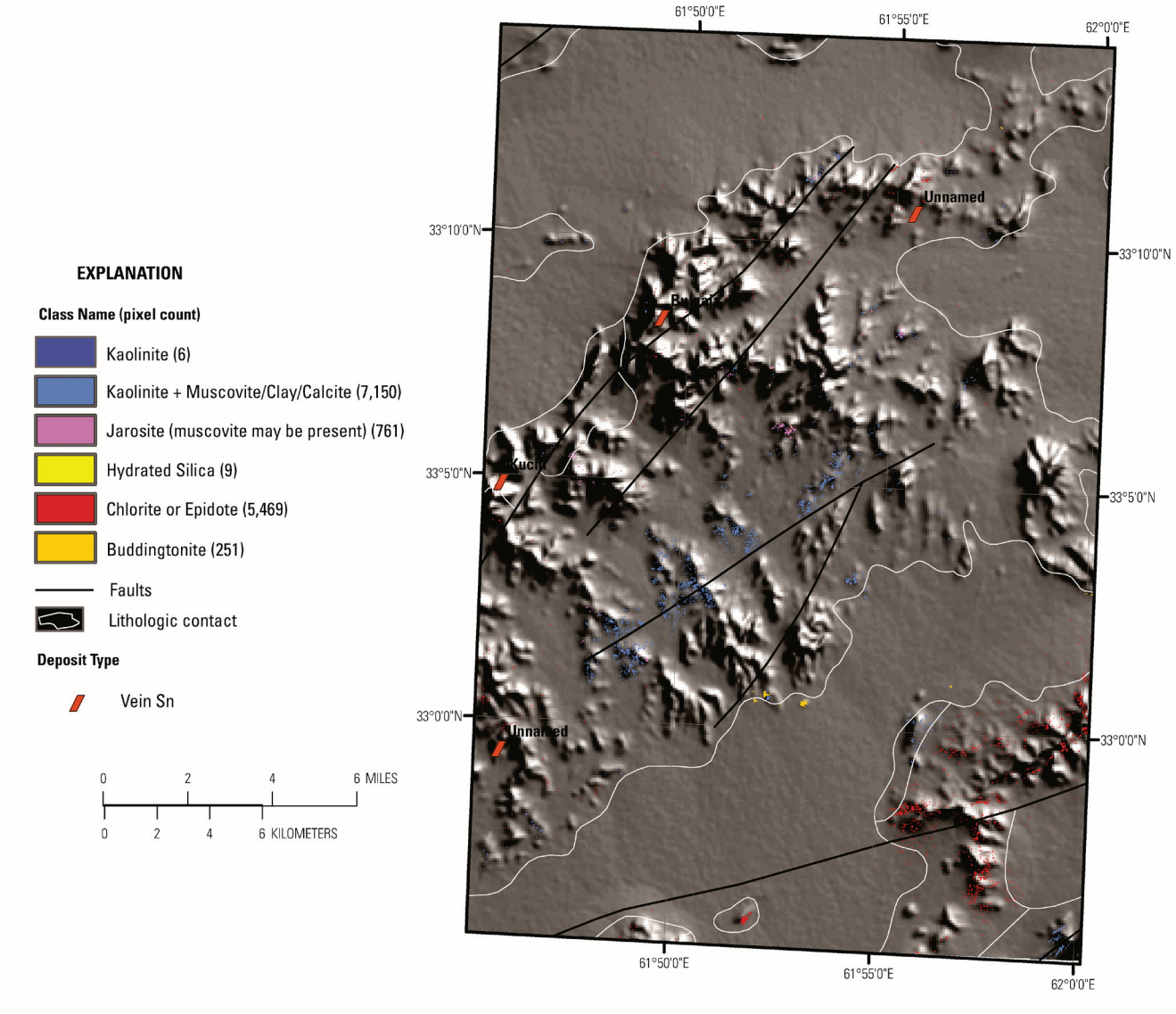

Figure 14B–12. Distribution of common alteration minerals in the Tourmaline area of interest.

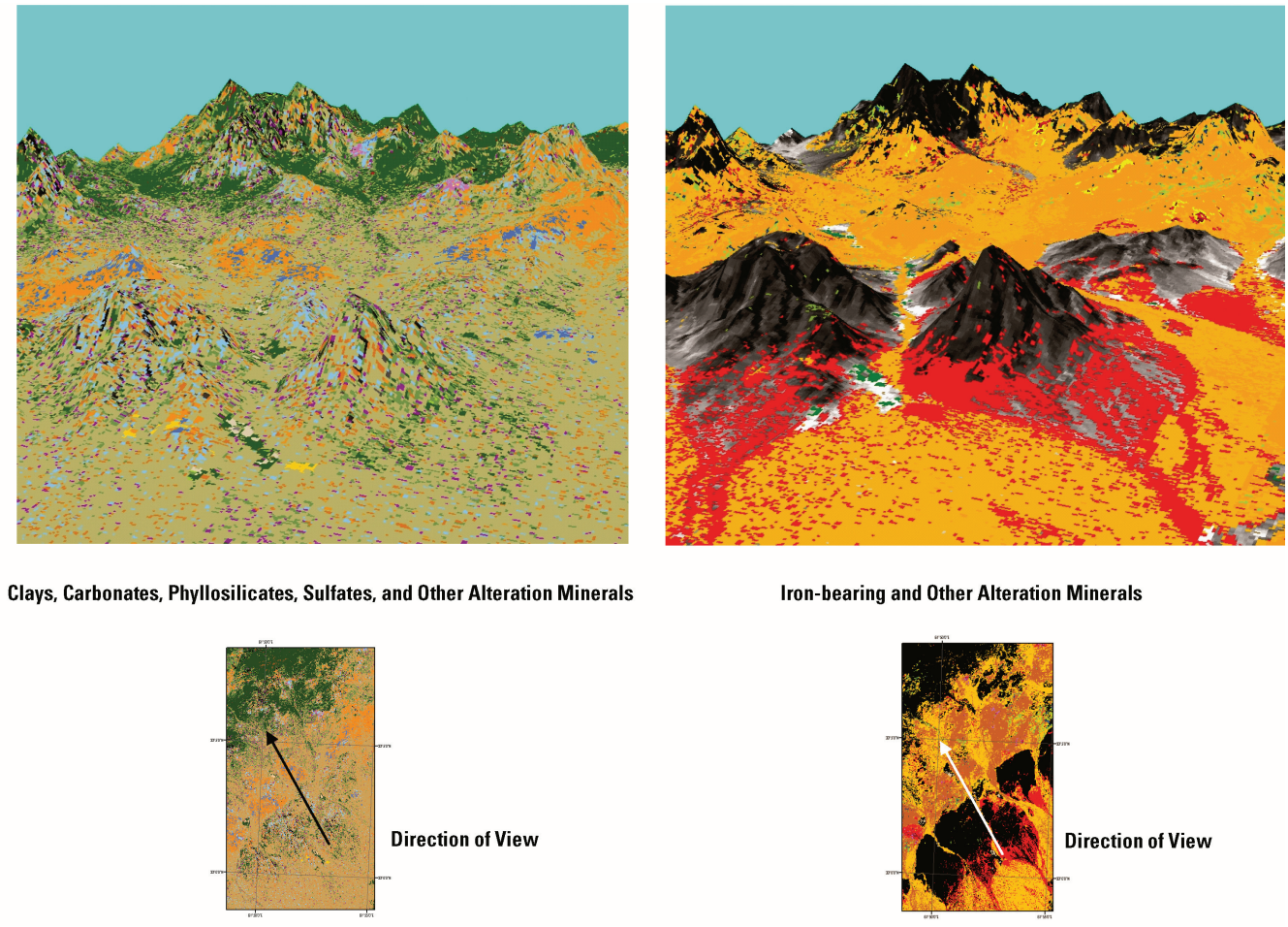

Figure 14B–13. A portion of figures 14B–6 (right) and 14B–7 (left) overlain on a DEM to produce a 3D depiction of a part of the Tourmaline area of interest. The color legends are the same as those in figures 14B–6 and 14B–7. The arrow shows the direction of the view relative to the map view images.

14B.6 References Cited

Abdullah, Sh., and Chmyriov, V.M., 1977, Geological map of Afghanistan: Kabul, Afghanistan, Ministry of Mining and Industry of the Democratic Republic of Afghanistan, scale 1:500,000.

Abdullah, Sh., Chmyriov, V.M., Stazhilo-Alekseev, K.F., Dronov, V.I., Gannan, P.J., Rossovskiy, L.N., Kafarskiy, A.Kh., and Malyarov, E.P., 1977, Mineral resources of Afghanistan (2d ed.): Kabul, Afghanistan, Republic of Afghanistan Geological and Mineral Survey, 419 p.

Cocks, T., Jenssen, R., Stewart, A., Wilson, I., and Shields, T., 1998, The HyMap airborne hyperspectral sensor—The system, calibration and performance, *in* Schaepman, M., Schlapfer, D., and Itten, K.I., eds., Proceedings of the 1st EARSeL Workshop on Imaging Spectroscopy, 6–8 October 1998, Zurich: Paris, European Association of Remote Sensing Laboratories, p. 37–43.

Davis, P.A., 2007, Landsat ETM+ false-color image mosaics of Afghanistan: U.S. Geological Survey Open-File Report 2007–1029, 22 p. (Also available at *http://pubs.usgs.gov/of/2007/1029/*.)

Doebrich, J.L., and Wahl, R.R., comps., *with contributions by* Doebrich, J.L., Wahl, R.R., Ludington, S.D., Chirico, P.G., Wandrey, C.J., Bohannon, R.G., Orris, G.J., Bliss, J.D., and ____, 2006, Geologic and mineral resource map of Afghanistan: U.S. Geological Survey Open File Report 2006–1038, scale 1:850,000, available at *http://pubs.usgs.gov/of/2006/1038/*.

Dronov, V.I., Kalimulin, S.M., Sborshchikov, I.M., Svezhentsov, V.P., Chistyakov, A.N., Zelensky, E.D., and Cherepov, P.G., 1972, The geology and minerals of North Afghanistan (parts of map sheets 400-II and 500-I, the Kaysar-Hari Rod Interfluve area): [Afghanistan] Department of Geological and Mineral Survey, 44 p.

Hoefen, T.M., Kokaly, R.F., and King, T.V.V., 2010, Calibration of HyMap data covering the country of Afghanistan, *in* Proceedings of the 15th Australasian Remote Sensing and Photogrammetry Conference, Alice Springs, Australia, September 12–17, 2010, p. 409, available at *http://dl.dropbox.com/u/81114/15ARSPC-Proceedings.zip/*.

King, T.V.V., Kokaly, R.F., Hoefen, T.M., and Knepper, D.H., 2010, Resource mapping in Afghanistan using HyMap data, *in* Proceedings of the 15th Australasian Remote Sensing and Photogrammetry Conference, Alice Springs, Australia, September 12–17, 2010, p. 500, available at *http://dl.dropbox.com/u/81114/15ARSPC-Proceedings.zip/*.

King, T.V.V., Kokaly, R.F., Hoefen, T.M., Dudek, K. and Livo, K.E., 2011, Surface materials map of Afghanistan—Iron-bearing minerals and other materials: U.S. Geological Survey Scientific Investigations Map 3152–B.

King, T.V.V., Johnson, M.R., Hoefen, T.M., Kokaly, R.F., and Livo, K.E., 2011, Mapping potential mineral resource anomalies using HyMap data, *in* King, T.V.V., Johnson, M.R., Hubbard, B.E., and Drenth, B.J., eds, Identification of mineral resources in Afghanistan—Detecting and mapping resource anomalies in prioritized areas using geophysical and remote sensing (ASTER and HyMap) data in Afghanistan: U.S. Geological Survey Open-File Report 2011–1229, available at *http://pubs.usgs.gov/of/2011/1229/*.

Kokaly, R.F., King, T.V.V., and Livo, K.E., 2008, Airborne hyperspectral survey of Afghanistan 2007—Flight line planning and HyMap data collection: U.S. Geological Survey Open-File Report 2008–1235, 14 p.

Kokaly, Ray, 2011, PRISM—Processing routines in IDL for spectroscopic measurements: U.S. Geological Survey Open-File Report 2011–1155, available at *http://pubs.usgs.gov/of/2011/1155/*.

Kokaly, R.F., King, T.V.V., Hoefen, T.M., Dudek, K. and Livo, K.E., 2011, Surface materials map of Afghanistan—Carbonates, phyllosilicates, sulfates, altered minerals, and other materials: U.S. Geological Survey Scientific Investigations Map 3152–A.

Peters, S.G., Ludington, S.D., Orris, G.J., Sutphin, D.M., Bliss, J.D., and Rytuba, J.J., eds., and the U.S. Geological Survey-Afghanistan Ministry of Mines Joint Mineral Resource Assessment Team, 2007, Preliminary non-fuel mineral resource assessment of Afghanistan: U.S. Geological Survey Open-File Report 2007–1214, 810 p., 1 CD–ROM. (Also available at *http://pubs.usgs.gov/of/2007/1214/*.)